

Effects of periodic kicking on dispersion and wave packet dynamics in graphene

Adhup Agarwala¹, Utso Bhattacharya², Amit Dutta², and Diptiman Sen³

¹*Department of Physics, Indian Institute of Science, Bengaluru 560012, India*

²*Department of Physics, Indian Institute of Technology, Kanpur 208016, India*

³*Centre for High Energy Physics, Indian Institute of Science, Bengaluru 560012, India*

We study the effects of δ -function periodic kicks on the Floquet energy-momentum dispersion in graphene. We find that a rich variety of dispersions can appear depending on the parameters of the kicking: at certain points in the Brillouin zone, the dispersion can become linear but anisotropic, linear in one direction and quadratic in the perpendicular direction, gapped with a quadratic dispersion, or completely flat (called dynamical localization). We show all these results analytically and demonstrate them numerically through the dynamics of wave packets propagating in graphene. We propose experimental methods for producing these effects.

PACS numbers: 05.70.Ln, 72.15.Rn

I. INTRODUCTION

Quantum systems driven periodically in time have been extensively studied in recent years from many points of view, such as the generation of defects^{1,2}, coherent destruction of tunneling^{3,4} and dynamical freezing⁵, dynamical saturation⁶ and localization⁷⁻⁹, dynamical fidelity¹⁰, edge singularity in the probability distribution of work¹¹ and thermalization¹² (see Ref. 13 for a review). These studies have become more important following the proposals of Floquet (irradiated) graphene¹⁴⁻¹⁶, Floquet topological insulators and the generation of topologically protected edge states¹⁷⁻³⁹; some of these aspects have been experimentally studied⁴⁰⁻⁴². We note that topologically ordered systems have also been studied using other driving schemes, for instance, sudden quenching; see Refs. 43-45.

Dynamical localization is a particularly interesting phenomenon; here the electrons become completely localized in space due to periodic driving of some parameter in the Hamiltonian. Examples of systems showing dynamical localization include driven two-level systems³, classical and quantum kicked rotors^{46,47}, the Kapitza pendulum⁴⁸, and bosons in an optical lattice⁴⁹.

There has been a tremendous amount of research on graphene in the last several years, both theoretical and experimental⁵⁰⁻⁵⁴. Graphene is a two-dimensional hexagonal lattice of carbon atoms in which the π electrons hop between nearest neighbors. The spectrum is gapless at two points (called \vec{K} and \vec{K}') in the Brillouin zone, and the energy-momentum dispersion around those points has the Dirac form $E_{\vec{k}} = \hbar v_F |\vec{k}|$, where $v_F \simeq 10^6 m/s$ is the Fermi velocity. The Dirac nature of the electrons gives rise to many interesting properties of this material. The ability to manipulate the dispersion of electrons in graphene can therefore be expected to give rise to some novel applications.

In this work, we will study the effects of periodic driving on an electron moving on the graphene lattice. We will use Floquet theory to look at the stroboscopic properties (i.e., measured at the end of each time period of

the driving) of the system. In particular we will be interested in the form of the quasi-energy dispersion and the dynamics of wave packets when various parameters in the Hamiltonian are given periodic δ -function kicks. (We note here that the effects of periodic kicking on charge transport and optical conductivity of a graphene nanoribbon have been studied in Ref. 55. Further, a proposal for using periodic pulses to simulate the effects of curvature in graphene has been made in Ref. 56). As we will see, the advantage of periodic δ -function kicks (in contrast to sinusoidal driving) is that the problem can be studied analytically to a large extent^{9,57}. We will show that for certain specific values of the driving parameters, the quasi-energy is completely independent of the momentum; this leads to zero group velocity and therefore to dynamical localization of wave packets. We also find other interesting phenomena. For example, the dispersion can become gapless along a particular line in the momentum space which results in a movement of wave packets along one particular direction in real space. We can also make the dispersion linear in one direction and quadratic in the perpendicular direction (called a semi-Dirac dispersion), or gapped and quadratic in both directions around certain points in the Brillouin zone.

The plan of our paper is as follows. In Sec. II, we recall the Hamiltonian and energy dispersion of graphene. In Sec. III, we describe the ideas of periodic δ -function kicking of the Hamiltonian and the quasi-energy dispersion for the most general form of kicking. Sec. IV describes how the dynamics of a Gaussian wave packet can be studied numerically. In Sec. V, we examine separately the effects of periodic kicking of three different parameters in the Hamiltonian. We show that a rich variety of quasi-energy dispersions can be obtained depending on the kicking parameters. The effects of these dispersions on the wave packet dynamics will be shown in some particularly interesting cases. In Sec. VI, we present a general way of understanding the phenomenon of dynamical localization. We end in Sec. VII with a summary of our main results, possible experimental realizations of periodic kicking of the different parameters, and some directions for future work.

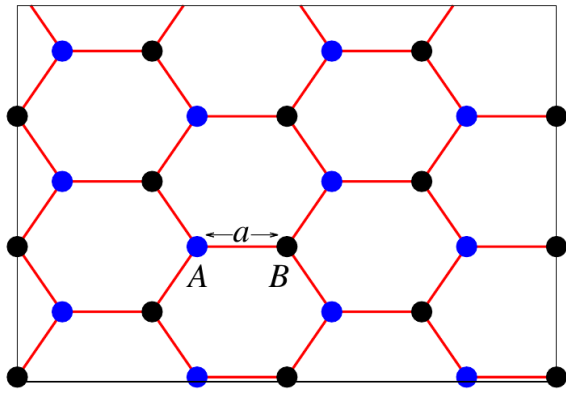


FIG. 1: The graphene lattice has a two-site unit cell; the sites are labeled A and B and are separated by a distance a .

II. HAMILTONIAN OF GRAPHENE

We begin with a brief description of the band structure of graphene. The Hamiltonian is given by a tight-binding model with nearest-neighbor hopping on a hexagonal lattice⁵¹

$$H = -\gamma \sum_{\vec{i}, \vec{j}} \sum_{s=\uparrow, \downarrow} (c_{\vec{i}, s}^\dagger c_{\vec{j}, s} + H.c.), \quad (1)$$

where the sum over \vec{i}, \vec{j} goes over the nearest neighbors (see Fig. 1), the hopping amplitude $\gamma \simeq 2.8$ eV, the nearest neighbor spacing is $a \simeq 0.14$ nm, and s denotes the spin component in, say, the z direction. (We will henceforth set $\hbar = 1$). Each unit cell of the hexagonal lattice consists of two sites; we denote the two sites, belonging to sublattices A and B , by $a_{\vec{n}}$ and $b_{\vec{n}}$ respectively. We introduce the Pauli matrices $\vec{\sigma}$ with $\sigma^z = \pm 1$ denoting sites on the A and B sublattices respectively. The midpoint of a unit cell labeled as \vec{n} is located at $\vec{n} = (3a/2)(n_1, (2n_2 + n_1)/\sqrt{3})$, where n_1, n_2 take integer values. The spanning vectors of the lattice are $\vec{M}_1 = (3a/2)(1, 1/\sqrt{3})$ and $\vec{M}_2 = (3a/2)(1, -1/\sqrt{3})$. The reciprocal lattice vectors can be chosen to be $\vec{G}_1 = (2\pi/3a)(1/2, \sqrt{3}/2)$ and $\vec{G}_2 = (2\pi/3a)(1/2, -\sqrt{3}/2)$.

In momentum space, the Hamiltonian in Eq. (1) takes the form

$$\begin{aligned} H_{\vec{k}} &= -\gamma \begin{pmatrix} 0 & 1 + e^{i\vec{k} \cdot \vec{M}_1} + e^{i\vec{k} \cdot \vec{M}_2} \\ 1 + e^{-i\vec{k} \cdot \vec{M}_1} + e^{-i\vec{k} \cdot \vec{M}_2} & 0 \end{pmatrix} \\ &= -\gamma (g_{\vec{k}} \sigma^x - h_{\vec{k}} \sigma^y), \end{aligned} \quad (2)$$

where

$$\begin{aligned} g_{\vec{k}} &= 1 + \cos(\vec{k} \cdot \vec{M}_1) + \cos(\vec{k} \cdot \vec{M}_2), \\ h_{\vec{k}} &= \sin(\vec{k} \cdot \vec{M}_1) + \sin(\vec{k} \cdot \vec{M}_2). \end{aligned} \quad (3)$$

As is well-known, the energy dispersion is given by $\pm E_{\vec{k}}$

where

$$\begin{aligned} E_{\vec{k}} &= \gamma \sqrt{g_{\vec{k}}^2 + h_{\vec{k}}^2} \\ &= \gamma [3 + 2 \cos(\sqrt{3}k_y a) + 4 \cos(\frac{\sqrt{3}k_y a}{2}) \cos(\frac{3k_x a}{2})]^{1/2}. \end{aligned} \quad (4)$$

The two bands touch each other at two inequivalent points; these are located at the wave vectors $\pm(0, 4\pi/(3\sqrt{3}a))$ and are called \vec{K} and \vec{K}' . Around these points, the effective low-energy continuum theory of graphene electrons takes the form of a two-dimensional Dirac Hamiltonian with

$$H_D = \sum_{\vec{k}} \psi_{\vec{k}}^\dagger [v_F (\sigma^x k_x + \tau^z \sigma^y k_y)] \psi_{\vec{k}}, \quad (5)$$

where $v_F = 3\gamma a/2$ is the Fermi velocity, $\tau^z = \pm 1$ at \vec{K} (\vec{K}') respectively (these are called valleys), and $\psi_{\vec{k}} \equiv \psi_{\vec{k}}^{\sigma\tau s}$ denote eight-component electron annihilation operators with the components corresponding to sublattice (σ), valley (τ), and spin (s) degrees of freedom. Equation (5) is the Dirac Hamiltonian and the dispersion is given by $\pm E_{\vec{k}} = \pm v_F |\vec{k}|$, with a four-fold degeneracy due to the valley and spin degrees of freedom. We will ignore the spin degree of freedom in this paper.

If we add a staggered potential of the form $f\sigma^z$, so that sites on the A and B sublattices have on-site energies f and $-f$ respectively, the Dirac Hamiltonian gets a mass f leading to the dispersion $\pm E_{\vec{k}} = \pm \sqrt{v_F^2 \vec{k}^2 + f^2}$; this has a gap of $2|f|$ at $\vec{k} = 0$.

In the next section we study what happens when various parameters in the Hamiltonian are given δ -function kicks with a time period T .

III. FLOQUET HAMILTONIAN FOR PERIODIC KICKING

We now apply δ -function kicks to the system, described by the following term in the Hamiltonian

$$H_{kick} = \sum_{\vec{n}} (\alpha_x \sigma^x + \alpha_y \sigma^y + \alpha_z \sigma^z) \sum_{m=-\infty}^{\infty} \delta(t - mT). \quad (6)$$

We assume that the periodic kicks are the same for all unit cells \vec{n} ; hence they add the term

$$H_{\vec{k}, kick} = (\alpha_x \sigma^x + \alpha_y \sigma^y + \alpha_z \sigma^z) \sum_{m=-\infty}^{\infty} \delta(t - mT) \quad (7)$$

to the momentum space Hamiltonian in Eq. (2).

The Floquet (stroboscopic) operator U_{XYZ} which evolves the system through one time period T is given by

$$U_{XYZ} = U_{\vec{k}, kick} U_{\vec{k}} = e^{-i\vec{\alpha} \cdot \vec{\sigma}} e^{-iH_{\vec{k}} T} \equiv e^{-iH_{XYZ} T} \quad (8)$$

in momentum space. This also defines for us the *effective* stroboscopic Hamiltonian H_{XYZ} . The eigenvalues of H_{XYZ} can be found by using the following identity for Pauli spin matrices,

$$e^{ia(\hat{n}\cdot\vec{\sigma})}e^{ib(\hat{m}\cdot\vec{\sigma})} = e^{ic(\hat{k}\cdot\vec{\sigma})}, \quad (9)$$

where $\{a, b, c\}$ are scalars and $\{\hat{n}, \hat{m}, \hat{k}\}$ are unit vectors. Here c and \hat{k} can be found in terms of a, b, \hat{n} and \hat{m} using the following relations:

$$\begin{aligned} \cos c &= \cos a \cos b - \hat{n} \cdot \hat{m} \sin a \sin b, \\ \hat{k} &= \frac{1}{\sin c} (\hat{n} \sin a \cos b + \hat{m} \sin b \cos a \\ &\quad - \hat{n} \times \hat{m} \sin a \sin b). \end{aligned} \quad (10)$$

Hence the eigenvalues of H_{XYZ} are equal to $\pm\varepsilon$, where the quasi-energy ε is given by

$$\begin{aligned} \varepsilon &= \frac{1}{T} \arccos [\cos \alpha \cos(E_{\vec{k}}T) \\ &\quad + \frac{\gamma(\alpha_x g_{\vec{k}} - \alpha_y h_{\vec{k}})}{\alpha E_{\vec{k}}} \sin \alpha \sin(E_{\vec{k}}T)] \end{aligned} \quad (11)$$

with $\alpha = \sqrt{\alpha_x^2 + \alpha_y^2 + \alpha_z^2}$. In the special case of only $\alpha_z \neq 0$, i.e., the kicking is applied to only the on-site energies of the graphene sublattice, the quasi-energy takes the particularly simple form $\varepsilon = \frac{1}{T} \arccos[\cos \alpha_z \cos(E_{\vec{k}}T)]$. We will discuss this in more detail below.

IV. WAVE PACKET DYNAMICS

To corroborate our results from the analytical results presented in the later sections, we numerically study the time evolution of a wave packet on the graphene lattice. We visualize the packet only at times which are integer multiples of T , consistent with our understanding of the effective dispersion given by ε .

Consider a wave packet $\vec{\Psi}$ in two spatial dimensions, with an initial momentum $\vec{k}_o = (k_{ox}, k_{oy})$ and a width σ . Namely,

$$\Psi(\vec{r}, t = 0) = \frac{1}{\sqrt{2\pi\sigma^2}} \exp\left(-\frac{r^2}{4\sigma^2}\right) \exp(i\vec{k}_o \cdot \vec{r}), \quad (12)$$

which is normalized such that $\int d\vec{r} |\Psi|^2 = 1$. The Fourier transform of Ψ is given by,

$$\Psi(\vec{k}, t = 0) = \sqrt{8\pi\sigma^2} \exp[-\sigma^2 \{(k_x - k_{ox})^2 + (k_y - k_{oy})^2\}]. \quad (13)$$

such that $\frac{1}{(2\pi)^2} \int dk_x dk_y |\Psi(\vec{k})|^2 = 1$.

Since the system has translational symmetry even in the presence of kicking, we can study the time evolution of each k mode separately. Thus a wave packet centered at \vec{k}_o can be evolved via U_{XYZ} and then Fourier transformed to the real space lattice. At each \vec{k} mode we have

a two-component vector associated with the occupancy of the graphene bands. Note that in the absence of any kicking, the upper and lower bands (positive and negative energies) have opposite velocities. Hence the wave packet movement will depend on the band which is initially occupied. In this work we always consider wave packets built out of the lower band (negative energy).

It may be useful to say a few words about our numerical procedure. We impose periodic boundary conditions in both real and momentum space. In momentum space, the Brillouin zone is a rhombus whose corners are at $(\pi/a)(-1/3, -1/\sqrt{3})$, $(\pi/a)(-1, 1/\sqrt{3})$, $(\pi/a)(1/3, 1/\sqrt{3})$, and $(\pi/a)(1, -1/\sqrt{3})$. If the number of unit cells is N^2 (the number of sites is $2N^2$), the real space lies in a rhombus whose center lies at $(0,0)$ and corners are at $(3aN/2)(-1/2, -\sqrt{3}/2)$, $(3aN/2)(1/2, -1/(2\sqrt{3}))$, $(3aN/2)(-1/2, 1/(2\sqrt{3}))$, and $(3aN/2)(1/2, \sqrt{3}/2)$. In Figs. 3 and 5, we have taken $a = 1$ and $N = 40$.

V. DISPERSION FOR UNIDIRECTIONAL KICKING

We now look at the effects of kicking in each of the three directions in the subsections below. We will show that kicks along σ^x , σ^y and σ^z can have quite different effects.

A. X-kicking: $\alpha_x \neq 0, \alpha_y = \alpha_z = 0$

We first consider the case when the kicking is applied only in the σ^x direction. In this case, we find that the quasi-energy spectrum given in Eq. (11) is gapless (i.e., $\varepsilon = 0$), when $h_{\vec{k}} = 0$, $E_{\vec{k}} = \gamma|g_{\vec{k}}|$, and $E_{\vec{k}}T = \alpha = |\alpha_x|$. This leads to the equations

$$\begin{aligned} 2 \cos\left(\frac{3k_x a}{2}\right) \cos\left(\frac{\sqrt{3}k_y a}{2}\right) &= \frac{\alpha_x}{\gamma T} - 1, \\ 2 \sin\left(\frac{3k_x a}{2}\right) \cos\left(\frac{\sqrt{3}k_y a}{2}\right) &= 0. \end{aligned} \quad (14)$$

This gives the following gapless points

$$\begin{aligned} \cos\left(\frac{\sqrt{3}k_y^g a}{2}\right) &= \frac{1}{2} \left(\frac{\alpha_x}{\gamma T} - 1\right), \\ \sin\left(\frac{3k_x^g a}{2}\right) &= 0. \end{aligned} \quad (15)$$

Clearly this can only be satisfied if $-\gamma T \leq \alpha_x \leq 3\gamma T$. We can also see that only k_y^g can be modulated using α_x . The low-energy dispersion about these gapless points can be found by expanding ε as follows,

$$\begin{aligned} \cos(\varepsilon T) &= \cos \alpha_x \cos(E_{\vec{k}}T) \\ &\quad + \left(1 - \frac{h_{\vec{k}}^2}{2g_{\vec{k}}^2}\right) \sin \alpha_x \sin(E_{\vec{k}}T), \end{aligned} \quad (16)$$

which implies that

$$\varepsilon^2 = \frac{1}{T^2} \left[(\alpha_x - E_{\vec{k}} T)^2 + \frac{\gamma^2 T^2 h_k^2}{\alpha_x^2} \sin^2 \alpha_x \right]. \quad (17)$$

The effective velocities about the gapless points are given by

$$\begin{aligned} v_x &= \frac{3a}{2T} \sqrt{\frac{(\alpha_x - \gamma T)^2 \sin^2 \alpha_x}{\alpha_x^2}}, \\ v_y &= \frac{3a}{2T} \sqrt{\frac{3\gamma^2 T^2 + 2\gamma T \alpha_x - \alpha_x^2}{3}}. \end{aligned} \quad (18)$$

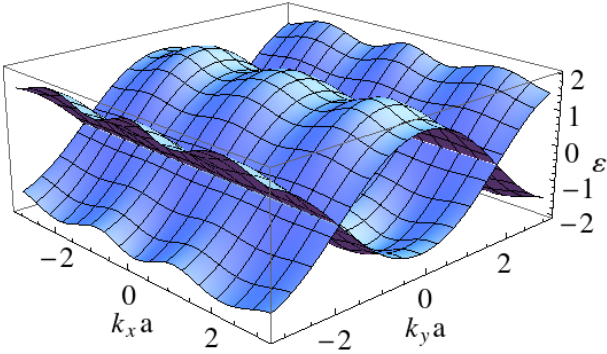


FIG. 2: Quasi-energy dispersion ε (in units of $1/T$) when $\alpha_x = \gamma T = 1$ and $\alpha_y = \alpha_z = 0$. There is a dispersionless line along the k_x direction when $k_y a = \pm\pi/\sqrt{3}$. A wave packet localized on this gapless line moves only in the y direction (see Fig. 3).

Interestingly, at the special value of $\alpha_x = \gamma T$, we obtain a dispersion which is gapless along k_x and disperses only along k_y at $k_y = k_y^g$. This dispersionless line is shown in Fig. 2, where we have chosen $\gamma T = 1$. Therefore a wave packet which is centered at $k_{oy} = k_y^g$ will move only in the y direction in real space in the presence of such a kicking. This is demonstrated in Fig. 3.

Another interesting case occurs as α_x is increased further. At $\alpha_x = 3\gamma T$, we find that the two Dirac points merge at $(k_x^g, k_y^g) = (0, 0)$ and we get a semi-Dirac dispersion there with $v_x = (a/T) \sin(3\gamma T)$ and $v_y = 0$. The dispersion is linear in k_x and quadratic in k_y , given by $\varepsilon = (3k_y^2 a^2 \gamma)/4$ for $k_x = 0$.

We would like to mention here that the merging of Dirac points in graphene resulting in a topological merging transition from a gapless to a gapped system has been studied extensively in recent years^{58–61}. Further, the same phenomenon has been studied inside the gapless phase of the Kitaev model on the hexagonal lattice in Ref. 62.

B. Y-kicking: $\alpha_y \neq 0, \alpha_x = \alpha_z = 0$

Next we consider the case when the kicking is applied only in the σ^y direction, i.e., $\alpha_y \neq 0$ and $\alpha_x = \alpha_z = 0$. Substituting the above values in Eq. (11), the gapless points are determined by $g_{\vec{k}} = 0$, $E_{\vec{k}} = \gamma |h_{\vec{k}}|$, and $E_{\vec{k}} T = |\alpha_y|$. We then get

$$\begin{aligned} 2 \cos\left(\frac{3k_x a}{2}\right) \cos\left(\frac{\sqrt{3}k_y a}{2}\right) &= -1, \\ 2 \sin\left(\frac{3k_x a}{2}\right) \cos\left(\frac{\sqrt{3}k_y a}{2}\right) &= -\frac{\alpha_y}{\gamma T}. \end{aligned} \quad (19)$$

These can be solved to obtain gapless points at (k_x^g, k_y^g) , where

$$\begin{aligned} \cos\left(\frac{\sqrt{3}k_y^g a}{2}\right) &= -\frac{1}{2} \sqrt{1 + \frac{\alpha_y^2}{\gamma^2 T^2}}, \\ \sin\left(\frac{3k_x^g a}{2}\right) &= \frac{\alpha_y}{\sqrt{\gamma^2 T^2 + \alpha_y^2}}. \end{aligned} \quad (20)$$

We see that a gapless point exists only if $|\alpha_y| \leq \sqrt{3}\gamma T$. In contrast to the earlier case with only $\alpha_x \neq 0$, both k_x^g and k_y^g can be modulated here using α_y .

Next we obtain the effective dispersion about these gapless points. Similar to the previous section, the low-energy expansion leads to

$$\begin{aligned} \cos(\varepsilon T) &= \cos \alpha_y \cos(E_{\vec{k}} T) \\ &+ \left(1 - \frac{g_{\vec{k}}^2}{2h_{\vec{k}}^2}\right) \sin \alpha_y \sin(E_{\vec{k}} T). \end{aligned} \quad (21)$$

Since the arguments of the both cosine terms are small, we expand both of them to obtain

$$\varepsilon^2 = \frac{1}{T^2} \left[(\alpha_y - E_{\vec{k}} T)^2 + \frac{\gamma^2 T^2 g_{\vec{k}}^2}{\alpha_y^2} \sin^2 \alpha_y \right]. \quad (22)$$

We see that the gapless points are Dirac-like and have anisotropic velocities given by

$$v_x = \frac{3a}{2T} \sqrt{\gamma^2 T^2 + \sin^2 \alpha_y}, \quad (23)$$

$$v_y = \frac{a}{T} \sqrt{\frac{3(3\gamma^2 T^2 - \alpha_y^2)(\gamma^2 T^2 \sin^2 \alpha_y + \alpha_y^4)}{4\alpha_y^2(\alpha_y^2 + \gamma^2 T^2)}}. \quad (24)$$

Interestingly, at $|\alpha_y| = \sqrt{3}\gamma T$, where the velocity v_y vanishes, we find a semi-Dirac dispersion which is linear in k_x but quadratic in the k_y direction; the low-energy dispersion in the k_y direction is given by

$$\varepsilon(k_x^g, k_y) = \frac{k_y^2 a^2}{T} \sqrt{\frac{3}{64} [9\gamma^2 T^2 + \sin^2(\sqrt{3}\gamma T)]}. \quad (25)$$

This is shown in Fig. 4, where we have chosen $\gamma T = 1$.

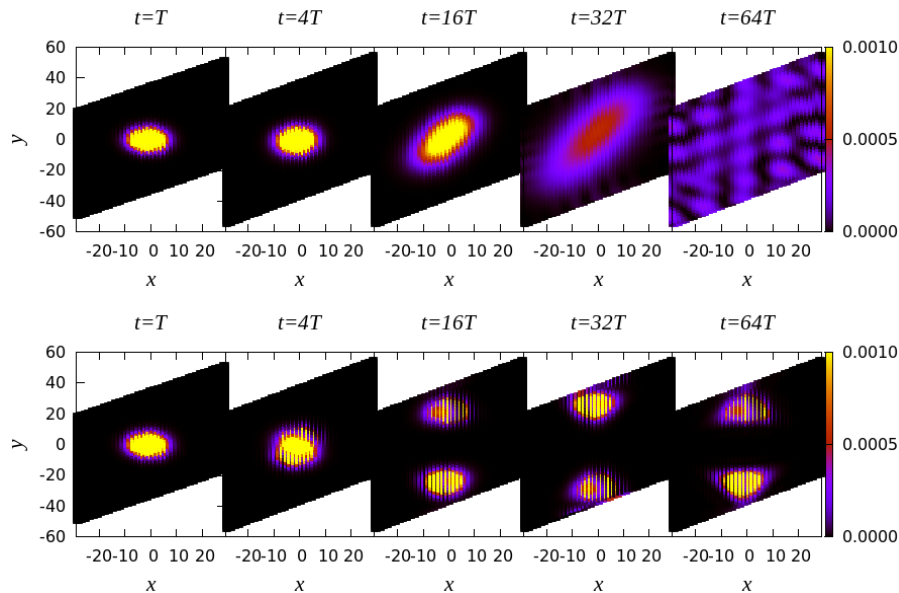


FIG. 3: Time evolution of a wave packet initially centered at $\vec{r} = (0, 0)$, at $t = T, 4T, 16T, 32T, 64T$ for no kicking (upper panel) and for $\alpha_x = \gamma T = 1$ and $\alpha_y = \alpha_z = 0$ (lower panel), with $k_{ox}a = 1$, $k_{oy}a = \frac{\pi}{\sqrt{3}}$ and $\sigma = \frac{10}{2\sqrt{2}}a$. The upper panel shows that in the absence of kicking the wave packet spreads out in both x and y directions. In the lower panel we see that the wave packet only moves in the y direction. This occurs because the wave packet is located at the dispersionless line in the k_x direction (see Fig. 2).

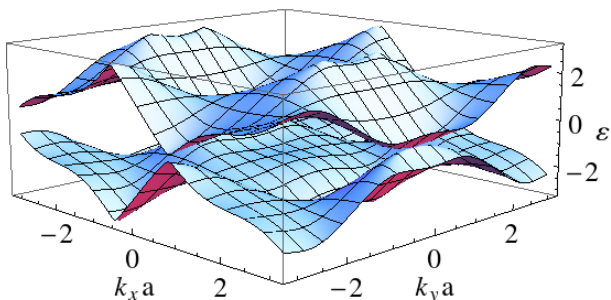


FIG. 4: Quasi-energy dispersion ε (in units of $1/T$) when $\alpha_y = \sqrt{3}\gamma T = \sqrt{3}$ and $\alpha_x = \alpha_z = 0$. While the dispersion is linear in the k_x direction, it is quadratic in the k_y direction near the gapless points (see text). This realizes a semi-Dirac dispersion.

C. Z-kicking: $\alpha_z \neq 0$, $\alpha_x = \alpha_y = 0$

Finally we consider a kicking which is applied in only the σ^z direction; this corresponds to applying a staggered potential on the A and B sublattices. The dispersion in

this case is given by

$$\varepsilon = \frac{1}{T} \arccos[\cos \alpha_z \cos(E_{\vec{k}} T)]. \quad (26)$$

At the Dirac points, $E_{\vec{k}} = 0$, we see that $\varepsilon = \alpha_z/T$; hence this kicking opens up a gap in the dispersion. Interestingly, at $\alpha_z = \pi/2$, we find that $\varepsilon = \pi/(2T)$, independent of the value of \vec{k} . Thus the dispersion becomes absolutely flat and therefore leads to dynamical localization. This is clearly shown in Fig. 5 where a wave packet gets localized in real space. Note that this is happening even though the system has no disorder and has translational symmetry.

At all other values of $\alpha_z \neq n\pi$ (where n is an integer), the original Dirac points at \vec{K} and \vec{K}' have a gap proportional to α_z/T and a low-energy dispersion which is quadratic in k . The effective dispersion is given by

$$\varepsilon = \frac{\alpha_z}{T} + \frac{1}{2} \cot \alpha_z E_{\vec{k}}^2 T. \quad (27)$$

VI. DYNAMICAL LOCALIZATION

In this section we will present a general understanding of dynamical localization due to periodic kicking. Suppose that there is a time-independent Hamiltonian H whose eigenstates and eigenvalues come in pairs, namely, ψ_j and ψ'_j with energies E_j and $-E_j$. Let us assume that there is a unitary operator P which produces this

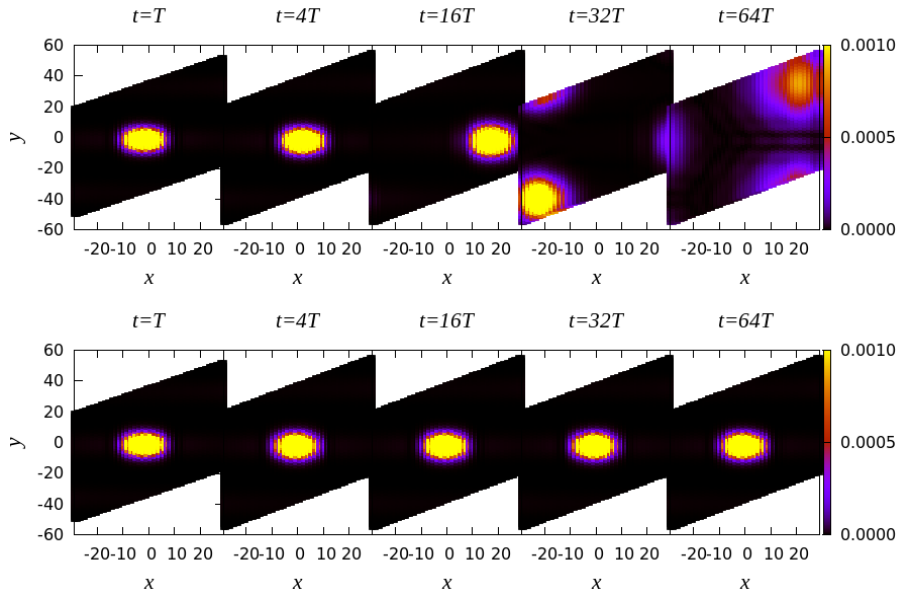


FIG. 5: Time evolution of a wave packet initially centered at $\vec{r} = (0, 0)$, at $t = T, 4T, 16T, 32T, 64T$ for no kicking (upper panel) and for $\alpha_z = \pi/2$ (lower panel), with $k_{ox}a = 1$ and $k_{oy}a = 0$ and $\sigma = \frac{10}{2\sqrt{2}}a$. The upper panel shows that the wave packet evolves with a net velocity in the x direction. The lower panel clearly demonstrates that the wave packet is localized. Notice that this happens in the absence of any disorder, so that translational symmetry is preserved. This is called dynamical localization.

transformation, namely, $PHP^{-1} = -H$, $P\psi_j = \psi'_j$ and $P\psi'_j = \psi_j$; hence $P^2 = I$. Then we can show as follows that a periodic kick with P will produce dynamical localization after two time periods. We begin with an eigenstate ψ_j and evolve it with the Hamiltonian H for a time T ; hence it picks up a phase e^{-iE_jT} . Then we kick it with P which converts it to the state ψ'_j . Upon evolving this with H for a time T , it picks up the phase e^{iE_jT} ; the two phases cancel each other exactly. Then another kick with P brings it back to the state ψ_j . Thus any eigenstate ψ_j will remain unchanged after a time $2T$. Since any state can be written as a superposition of eigenstates of H , we see that any state will remain the same after a time $2T$; this implies dynamical localization.

For any bipartite lattice with hopping only between sites belonging to different sublattices (graphene is a special case of this), we can see that an operator P which changes the phase of an eigenstate on only one sublattice by -1 produces another eigenstate with the opposite energy. A kick with a staggered potential of strength $\pi/2$ is precisely equivalent to such an operator P (up to an overall phase of i). This explains why we observe dynamical localization when $\alpha_z = \pi/2$ and $\alpha_x = \alpha_y = 0$. In fact, dynamical localization will occur even if we consider a finite piece of graphene with an arbitrary size and shape.

VII. CONCLUDING REMARKS

We have shown that applying δ -function kicks in different directions in the sublattice space in graphene can lead to interesting physics including dispersionless lines in momentum space, semi-Dirac dispersion and even a completely flat dispersion. We have shown that these lead to rich possibilities for the time evolution of wave packets, such as motion along only one direction or a complete dynamical localization. Given the widespread interest in graphene, the ability to tune its dispersion and obtain a range of dynamical behaviors should lead to applications in a variety of settings.

We note that a dynamical localization-to-delocalization transition has been observed in a quantum kicked rotor. Such a system is realized by placing cold atoms in a pulsed, far-detuned, standing wave, and the transition is detected by measuring the number of zero velocity atoms under the influence of a quasi-periodic driving⁶³.

We would like to mention possible experimental realizations of periodic driving of a graphene system.

(i) If a metallic sheet carrying a uniform current in the x direction is placed parallel to the graphene (but displaced from it by some distance in the z direction), this produces a constant magnetic field in the y direction. The corresponding vector potential can be chosen to be in the x direction with a magnitude which is linear in the z coordinate. Hence it will be a constant vector in the graphene plane. This vector potential can be introduced

as a Peierls phase in the nearest neighbor hoppings. If we now vary the current periodically in time, we will have a periodically varying hopping phase which cannot be removed by a global gauge transformation. This provides a possible experimental route to achieve the temporal driving in the σ^x and σ^y directions that we have studied in this paper.

(ii) A kicking proportional to σ^z can be experimentally set up as follows. h-BN (a form of boron nitride with a hexagonal lattice structure) and graphene have lattice spacings which are nearly equal; hence one of them can be placed on the other. The boron and nitrogen atoms exert different van der Waals forces on the two graphene carbon atoms in an unit cell, thus creating an effective sublattice potential⁶⁴. A periodic application of the pressure on these two layers (from the top and the bottom) should modulate the distance between the layers and thus lead to a periodic modulation of the sublattice potential.

Finally, we point out some possible directions for future studies. One can study what kinds of edge states can be generated in graphene by periodic kicking of different kinds. In the absence of kicking, it is known that graphene has states on a zigzag edge but not on an armchair edge^{65,66}. It would be interesting to know if pe-

riodic driving can change this situation, as is known to happen in the Kitaev model on the hexagonal lattice³⁹. It would also be very interesting to analyze the effects of interactions in periodically kicked graphene. One of the central results of this paper is that at $\alpha_z = \pi/2$ the quasi-energy spectrum becomes completely dispersionless. Under these conditions any interaction energy scale in the problem will be dominant due to quenching of the “effective” kinetic energy. It can therefore be intriguing to understand the stroboscopic evolution of a many-particle state in such a system. The presence of a highly anisotropic Dirac dispersion and dispersionless lines in the spectrum may also produce exotic many-body phases in the presence of interactions.

Acknowledgments

We thank Arnab Das for interesting discussions. A.A. thanks CSIR, India for funding through a SRF fellowship. A.D. thanks DST, India for Project No. SB/S2/CMP-19/2013 and D.S. thanks DST, India for Project No. SR/S2/JCB-44/2010 for financial support.

-
- ¹ V. Mukherjee, A. Dutta, and D. Sen, Phys. Rev. B **77**, 214427 (2008).
 - ² V. Mukherjee and A. Dutta, J. Stat. Mech. (2009) P05005.
 - ³ F. Grossmann, T. Dittrich, P. Jung, and P. Hänggi, Phys. Rev. Lett. **67**, 516 (1991).
 - ⁴ Y. Kayanuma, Phys. Rev. A **50**, 843 (1994).
 - ⁵ A. Das, Phys. Rev. B **82**, 172402 (2010).
 - ⁶ A. Russomanno, A. Silva, and G. E. Santoro, Phys. Rev. Lett. **109**, 257201 (2012).
 - ⁷ L. D’Alessio and A. Polkovnikov, Ann. Phys. (N.Y.) **333**, 19 (2013).
 - ⁸ M. Bukov, L. D’Alessio, and A. Polkovnikov, Advances in Physics **64**, 139 (2015).
 - ⁹ T. Nag, S. Roy, A. Dutta, and D. Sen, Phys. Rev. B **89**, 165425 (2014).
 - ¹⁰ S. Sharma, A. Russomanno, G. E. Santoro, and A. Dutta, EPL **106**, 67003 (2014).
 - ¹¹ A. Russomanno, S. Sharma, A. Dutta and G. E. Santoro, J. Stat. Mech. (2015) P08030.
 - ¹² A. Lazarides, A. Das, and R. Moessner, Phys. Rev. Lett. **112**, 150401 (2014).
 - ¹³ A. Dutta, G. Aeppli, B. K. Chakrabarti, U. Divakaran, T. Rosenbaum and D. Sen, *Quantum Phase Transitions in Transverse Field Spin Models: From Statistical Physics to Quantum Information* (Cambridge University Press, Cambridge, 2015).
 - ¹⁴ Z. Gu, H. A. Fertig, D. P. Arovas, and A. Auerbach, Phys. Rev. Lett. **107**, 216601 (2011).
 - ¹⁵ T. Kitagawa, T. Oka, A. Brataas, L. Fu, and E. Demler, Phys. Rev. B **84**, 235108 (2011).
 - ¹⁶ E. Suárez Morell and L. E. F. Foa Torres, Phys. Rev. B **86**, 125449 (2012).
 - ¹⁷ T. Kitagawa, E. Berg, M. Rudner, and E. Demler, Phys. Rev. B **82**, 235114 (2010).
 - ¹⁸ N. H. Lindner, G. Refael, and V. Galitski, Nature Phys. **7**, 490 (2011).
 - ¹⁹ L. Jiang, T. Kitagawa, J. Alicea, A. R. Akhmerov, D. Pekker, G. Refael, J. I. Cirac, E. Demler, M. D. Lukin, and P. Zoller, Phys. Rev. Lett. **106**, 220402 (2011).
 - ²⁰ M. Trif and Y. Tserkovnyak, Phys. Rev. Lett. **109**, 257002 (2012).
 - ²¹ A. Gomez-Leon and G. Platero, Phys. Rev. B **86**, 115318 (2012), and Phys. Rev. Lett. **110**, 200403 (2013).
 - ²² B. Dóra, J. Cayssol, F. Simon, and R. Moessner, Phys. Rev. Lett. **108**, 056602 (2012).
 - ²³ J. Cayssol, B. Dora, F. Simon, and R. Moessner, Phys. Status Solidi RRL **7**, 101 (2013).
 - ²⁴ D. E. Liu, A. Levchenko, and H. U. Baranger, Phys. Rev. Lett. **111**, 047002 (2013).
 - ²⁵ Q.-J. Tong, J.-H. An, J. Gong, H.-G. Luo, and C. H. Oh, Phys. Rev. B **87**, 201109(R) (2013).
 - ²⁶ M. S. Rudner, N. H. Lindner, E. Berg, and M. Levin, Phys. Rev. X **3**, 031005 (2013).
 - ²⁷ Y. T. Katan and D. Podolsky, Phys. Rev. Lett. **110**, 016802 (2013).
 - ²⁸ N. H. Lindner, D. L. Bergman, G. Refael, and V. Galitski, Phys. Rev. B **87**, 235131 (2013).
 - ²⁹ A. Kundu and B. Seradjeh, Phys. Rev. Lett. **111**, 136402 (2013).
 - ³⁰ V. M. Bastidas, C. Emary, G. Schaller, A. Gómez-León, G. Platero, and T. Brandes, arXiv:1302.0781v2.
 - ³¹ T. L. Schmidt, A. Nunnenkamp, and C. Bruder, New J. Phys. **15**, 025043 (2013).
 - ³² A. A. Reynoso and D. Frustaglia, Phys. Rev. B **87**, 115420 (2013).
 - ³³ C.-C. Wu, J. Sun, F.-J. Huang, Y.-D. Li, and W.-M. Liu,

- EPL **104**, 27004 (2013).
- ³⁴ M. Thakurathi, A. A. Patel, D. Sen, and A. Dutta, Phys. Rev. B **88**, 155133 (2013).
- ³⁵ P. M. Perez-Piskunow, G. Usaj, C. A. Balseiro, and L. E. F. Foa Torres, Phys. Rev. B **89**, 121401(R) (2014).
- ³⁶ G. Usaj, P. M. Perez-Piskunow, L. E. F. Foa Torres, and C. A. Balseiro, Phys. Rev. B **90**, 115423 (2014).
- ³⁷ P. M. Perez-Piskunow, L. E. F. Foa Torres, and G. Usaj, Phys. Rev. A **91**, 043625 (2015).
- ³⁸ M. D. Reichl and E. J. Mueller, Phys. Rev. A **89**, 063628 (2014).
- ³⁹ M. Thakurathi, K. Sengupta, and D. Sen, Phys. Rev. B **89**, 235434 (2014).
- ⁴⁰ T. Kitagawa, M. A. Broome, A. Fedrizzi, M. S. Rudner, E. Berg, I. Kassal, A. Aspuru-Guzik, E. Demler, and A. G. White, Nat. Commun. **3**, 882 (2012).
- ⁴¹ M. C. Rechtsman, J. M. Zeuner, Y. Plotnik, Y. Lumer, D. Podolsky, S. Nolte, F. Dreisow, M. Segev, and A. Szameit, Nature (London) **496**, 196 (2013); M. C. Rechtsman, Y. Plotnik, J. M. Zeuner, D. Song, Z. Chen, A. Szameit, and M. Segev, Phys. Rev. Lett. **111**, 103901 (2013).
- ⁴² G. Puentes, I. Gerhardt, F. Katzschmann, C. Silberhorn, J. Wrachtrup, and M. Lewenstein, Phys. Rev. Lett. **112**, 120502 (2014).
- ⁴³ A. A. Patel, S. Sharma, and A. Dutta, Eur. Phys. J B **86**, 367 (2013).
- ⁴⁴ A. Rajak, T. Nag, and A. Dutta, Phys. Rev. E **90**, 042107 (2014).
- ⁴⁵ P. D. Sacramento, Phys. Rev. E **90**, 032138 (2014).
- ⁴⁶ B. V. Chirikov, F. M. Izrailev, and D. L. Shepelyansky, Sov. Sci. Rev. **C 2**, 209 (1981); S. Fishman, D. R. Grempel, and R. E. Prange, Phys. Rev. Lett. **49**, 509 (1982).
- ⁴⁷ H. Ammann, R. Gray, I. Shvarchuck, and N. Christensen, Phys. Rev. Lett. **80**, 4111 (1998).
- ⁴⁸ P. L. Kapitza, Sov. Phys. JETP **21**, 588 (1951); H. W. Broer, I. Hoveijn, M. van Noort, C. Simon, and G. Vegter, Journal of Dynamics and Differential Equations, **16** 897 (2004).
- ⁴⁹ B. Horstmann, J. I. Cirac, and T. Roscilde, Phys. Rev. A **76**, 043625 (2007).
- ⁵⁰ C. W. J. Beenakker, Rev. Mod. Phys. **80**, 1337 (2008).
- ⁵¹ A. H. Castro Neto, F. Guinea, N. M. R. Peres, K. S. Novoselov, and A. K. Geim, Rev. Mod. Phys. **81**, 109 (2009).
- ⁵² S. Das Sarma, S. Adam, E. H. Hwang, and E. Rossi, Rev. Mod. Phys. **83**, 407 (2011).
- ⁵³ M. O. Goerbig, Rev. Mod. Phys. **83**, 1193 (2011).
- ⁵⁴ D. N. Basov, M. M. Fogler, A. Lanzara, F. Wang, and Y. Zhang, Rev. Mod. Phys. **86**, 959 (2014).
- ⁵⁵ D. Babajanov, D. U. Matrasulov, and R. Egger, Eur. Phys. J. B **87**, 258 (2014).
- ⁵⁶ T. Mishra, T. Guha Sarkar, and J. N. Bandyopadhyaya, Eur. Phys. J. B **88**, 231 (2015).
- ⁵⁷ S. Dasgupta, U. Bhattacharya, and A. Dutta, Phys. Rev. E **91**, 052129 (2015).
- ⁵⁸ S. Koghee, L.-K. Lim, M. O. Goerbig, and C. M. Smith, Phys. Rev. A **85**, 023637 (2012).
- ⁵⁹ P. Delplace, D. Ullmo, and G. Montambaux, Phys. Rev. B **84**, 195452 (2011).
- ⁶⁰ L.-K. Lim, J.-N. Fuchs, and G. Montambaux, Phys. Rev. Lett. **108**, 175303 (2012).
- ⁶¹ P. Delplace, A. Gomez-Leon, and G. Platero, Phys. Rev. B **88**, 245422 (2013).
- ⁶² U. Bhattacharya, S. Dasgupta, and A. Dutta, arXiv:1508.04598v3.
- ⁶³ J. Ringot, P. Szczytko, J. C. Garreau, and D. Delande, Phys. Rev. Lett. **85**, 2741 (2000).
- ⁶⁴ J. Jung, A. M. DaSilva, A. H. MacDonald, and S. Adam, Nature Commun. **6**, 6308 (2015).
- ⁶⁵ K. Nakada, M. Fujita, G. Dresselhaus, and M. S. Dresselhaus, Phys. Rev. B **54**, 17954 (1996).
- ⁶⁶ M. Kohmoto and Y. Hasegawa, Phys. Rev. B **76**, 205402 (2007).